Received: 8 February 2022 | Accepted: 12 July 2022

DOI: 10.1002/jcp.30840

RESEARCH ARTICLE

Journal of Cellular Physiology WILEY

# Oxygen gradients dictate angiogenesis but not barriergenesis in a 3D brain microvascular model

Kiet A. Tran | Abigail Baldwin-Leclair | Brandon J. DeOre | Morgan Antisell | Peter A. Galie

Department of Biomedical Engineering, Rowan University, Glassboro, New Jersey, USA

**Correspondence**
Peter A. Galie, Department of Biomedical Engineering, Rowan University, Glassboro, NJ, USA.
Email: galie@rowan.edu

**Funding information**
National Science Foundation, Grant/Award Number: 2034780

## Abstract

A variety of biophysical properties are known to regulate angiogenic sprouting, and in vitro systems can parse the individual effects of these factors in a controlled setting. Here, a three-dimensional brain microvascular model interrogates how variables including extracellular matrix composition, fluid shear stress, and radius of curvature affect angiogenic sprouting of cerebral endothelial cells. Tracking endothelial migration over several days reveals that application of fluid shear stress and enlarged vessel radius of curvature both attenuate sprouting. Computational modeling informed by oxygen consumption assays suggests that sprouting correlates to reduced oxygen concentration: both fluid shear stress and vessel geometry alter the local oxygen levels dictated by both ambient conditions and cellular respiration. Moreover, increasing cell density and consequently lowering the local oxygen levels yields significantly more sprouting. Further analysis reveals that the magnitude of oxygen concentration is not as important as its spatial concentration gradient: decreasing ambient oxygen concentration causes significantly less sprouting than applying an external oxygen gradient to the vessels. In contrast, barriergenesis is dictated by shear stress independent of local oxygen concentrations, suggesting that different mechanisms mediate angiogenesis and barrier formation and that angiogenic sprouting can occur without compromising the barrier. Overall, these results improve our understanding of how specific biophysical variables regulate the function and activation of cerebral vasculature, and identify spatial oxygen gradients as the driving factor of angiogenesis in the brain.

**KEYWORDS**
angiogenesis, barriergenesis, hypoxia, oxygen gradients, shear stress

## 1 | INTRODUCTION

The brain is a highly metabolically active organ that accounts for 20% of the body's total oxygen consumption despite only accounting for approximately 2% of total body weight (Rink & Khanna, 2011). It has a heterogeneous topography of local metabolic requirements dictated by neuronal density and activity (Watts et al., 2018), and precise regulation of blood flow to supply oxygen and nutrients is vital for proper functioning of brain tissue. While most endothelial cell subtypes in other parts of the body rely heavily on glycolysis for energy production (Caja & Enríquez, 2017), cerebral endothelial cells, which form tight junctions that give rise to the blood-brain barrier,

Kiet A. Tran and Abigail Baldwin-LeClair contributed equally to this study.

  

contain a greater concentration of mitochondria that produce energy via oxidative phosphorylation (Yetkin-Arik et al., 2019). This difference suggests that cerebral endothelial cells may be more sensitive to changes in local oxygen concentrations than in other tissues. Recent studies have shown that even mild levels of hypoxia can lead to blood-brain barrier disruption and subsequent angiogenesis in mice (Halder & Milner, 2020), but the relationship between oxygen tension and cerebral endothelial function has yet to be directly interrogated in a controlled, in vitro environment.

Hypoxia occurs in physiological processes including development as well as a broad range of pathologies that encompasses cancer and stroke (Hickey & Simon, 2006). Hypoxia is generally associated with an increase in angiogenesis through activation of hypoxia inducible factors, which in turn regulate the transcription of proangiogenic factors (Doddaballapur et al., 2015). In systemic vasculature, and specifically during processes related to cancer, angiogenesis is generally associated with increased vascular permeability due to the effects of proteins like vascular endothelial growth factor (VEGF) (Niu & Chen, 2010). However, increased permeability in the brain has severe consequences: blood-brain barrier disruption leads to inflammation and subsequent damage to the surrounding parenchyma (Clifford et al., 2007). Previous studies have shown that angiogenesis and barriergenesis can occur simultaneously in the developing brain so that new blood vessels can sprout from existing vasculature without allowing transport of blood components into the extracellular matrix of the central nervous system (Umans et al., 2017). However, the factors that mediate angiogenesis and barriergenesis in cerebral vasculature during both development and disease remain mostly unclear.

In recent years, in vitro models of vasculature have provided tremendous insight into angiogenesis and the formation of neovasculature in controlled, three-dimensional environments. In contrast to tubulogenesis assays on two-dimensional substrates, 3D systems can capture the cell-matrix interactions that mediate sprouting and neovessel formation. The effects of both biochemical factors (Nguyen et al., 2013, 2017; van Duinen et al., 2019) and mechanical stimuli (Galie et al., 2014; Kim et al., 2016; Lee et al., 2022; Polacheck et al., 2019; Song et al., 2012; Wang, Jarman, et al., 2021; Wang, Kent, et al., 2021; Winkelman et al., 2022) on angiogenesis have been extensively investigated in these systems. The primary advantage of 3D models, despite not fully recapitulating the in vivo microenvironment, is their ability to precisely control environmental factors to provide a mechanistic understanding of proangiogenic processes. These systems have also been used to assess the angiogenic response to hypoxia (Williams et al., 2015), demonstrating that hypoxia influences the effects of other factors that stimulate neovessel formation. The recent development of 3D models of the blood-brain barrier provides a means to interrogate the effect of hypoxia and other factors on both angiogenesis and barriergenesis in a controlled environment.

Another advantage of 3D in vitro models is their compatibility with computational modeling to predict spatial and temporal distributions of angiogenic factors exposed to endothelialized vessels. Complex computational models have been developed to predict the angiogenic response to interstitial fluid flow by coupling convective and diffusive transport with constitutive equations predicting cell division and migration (Alberding & Secomb, 2021; Hormuth et al., 2021; Polacheck et al., 2019; Vilanova et al., 2018). Coupling finite element simulations of oxygen transport with experimental data has previously been used to predict cell viability within in vitro systems (Bowers et al., 2019). An important component of oxygen tension models is the prediction of cellular oxygen consumption, which serves as a major sink in the diffusive constitutive equation. There has been substantial innovation in systems to directly measure cellular oxygen consumption including microfluidic-based approaches (Azimzadeh et al., 2021). Accurate measurements of oxygen consumption are vital to informing computational models of oxygen diffusion within in vitro systems, and previous studies have provided measurements of oxygen consumption by cerebral endothelial cells in culture (McDonald et al., 2019; Rellick et al., 2016; Sheikh et al., 2020). Overall, combining in vitro platforms with computational models informed by cellular oxygen consumption rates can provide new insight into processes affecting angiogenesis and barriergenesis in cerebral vasculature.

## 2 | MATERIALS AND METHODS

### 2.1 | Microfabricated devices and hydrogel preparation

Polydimethylsiloxane (PDMS) microfluidic devices were fabricated using soft lithography (DeOre et al., 2022; Partyka et al., 2017). Briefly, positive features were used to cast negative features and a layer of PDMS was used to enclose the devices. The hydrogel reservoir was filled with 5 M sulfuric acid for 90 min, washed thoroughly with deionized water, and coated with 20 μg/ml collagen for 60 min. All microfluidic devices were sterilized using shortwave length ultraviolet light before use. Collagen hydrogels were formed within reservoirs in the device by mixing solubilized collagen in 0.02 N acetic acid with 10X PBS, 0.1 M NaOH, 1 mg/ml of Matrigel and deionized water to yield a final concentration of 2 mg/ml (Bowers et al., 2019; Galie et al., 2015). For gels containing hyaluronan (HA), the deionized water was replaced with 2–2.4 MDa HA to create a final mixture of 1 mg/ml HA, 1 mg/ml Matrigel, and 2 mg/ml collagen (DeOre et al., 2022; Placone et al., 2015).

### 2.2 | Cell culture

P22-23 human cerebral microvascular endothelial cells (HCMEC/d3) were cultured in gelatin-coated culture plates before use in experiments. Modified endothelial growth medium (EGM-2) was prepared using a previous protocol (Weksler, 2005). The final concentrations of EGM-2 yielded the following: 5 μg/ml ascorbic

acid (Sigma), 1 ng/ml bFGF (Peprotech), 1% chemically defined lipid concentration (Thermo Fisher) 5% fetal bovine serum (FBS) (VWR), 10 mM HEPES buffer (VWR), 1.4 µM of hydrocortisone (VWR), and 1% penicillin-streptomycin (VWR). HCMEC/d3 were thawed 5 days before seeding and medium was changed every other day.

## 2.3 | 3D angiogenic model

Three-dimensional blood vessels were fabricated using a previously described protocol (DeOre et al., 2022; Partyka et al., 2017). Briefly, 60 µl of collagen gel was injected into the hydrogel reservoir of the device and either 180-µm or 300-µm diameter acupuncture needles coated with 0.1% BSA were inserted before polymerization. The needles were removed after the hydrogel polymerized to create 2 parallel cylindrical channels in which HCMEC/d3 cells were injected into one channel at a density of $5 \times 10^6$ cells/ml. For high-density 300-µm blood vessels, cells were seeded at a density of $20 \times 10^6$ cells/ml. The endothelialized channels were incubated for 10 min on each side to ensure cell attachment. Following cell seeding, these channels were either exposed to static conditions or perfused with culture medium using a linear syringe pump (Kent Scientific) for 4 days.

## 2.4 | Hypoxia experiments

Blood vessels fabricated in 300-µm channels were cultured with EGM-2 in static conditions in a 1% $O_2$ hypoxic chamber by purging with nitrogen for 4 days while maintaining 37°C and 5% $CO_2$. To create an oxygen gradient in a hypoxic incubator, a syringe pump containing EGM-2 was placed outside the incubator and injected the medium into the adjacent channel at a fixed rate of 2.4 µl/min for 4 days.

## 2.5 | Immunocytochemistry

Microfluidic devices were fixed with 4% paraformaldehyde (Alfa Aesar) for 20 min and permeabilized with 0.2% Triton X-100 (Sigma) for 20 min at room temperature. For ZO-1 labeling, hydrogels were removed from the devices and blocked by 3% bovine serum albumin (BSA) for 30 min at room temperature. These gels were incubated with 1:250 anti-ZO-1 (Cell Signaling) for 48 h at 4°C. These gels were washed thoroughly with PBS and all secondary antibodies were used at 1:500 dilution. Cell nuclei were identified with 4′,6-diamidino-2-phenylindole (DAPI) (1:500) and F-actin was stained using Alexa Fluor 488-conjugated phalloidin at 37°C for 60 min.

## 2.6 | Sprout quantification

Images of the vessel walls were converted to 8-bit image files, rotated, and cropped to a height of 999.81 units so that the sprouts emanated from the right side of the image. A custom MATLAB program converted the image to a binary matrix with a gradient mask. Based on the final binary mask image, a new matrix was generated. The sprout frequency for each vessel wall was determined by calculating the percentage of the vessel border exceeding a threshold distance of 40 microns from the parent microvessel to include only mature sprouts. The algorithm was also utilized to evaluate the normalized average sprout length, standard deviation, root mean square, and maximum length of the sprouting in each vessel wall.

## 2.7 | Glucose measurements

To measure the glucose concentrations within each vessel condition, 15-µl of media was removed from 300-µm diameter vessels (both low and high density) after 4 days of incubation. Test strips compatible with a OneTouch glucometer were used to determine the amounts of glucose in the media and measurements were performed in triplicates for each condition.

## 2.8 | Permeability testing

Blood vessels exposed to experimental conditions were transferred to a stage of an inverted epifluorescent microscope enclosed by an environmental chamber. Using a syringe pump, 4-kDa FITC dextran was perfused into the channels at a flow rate of 5 µl/min for 10 min while submerged in culture medium to maintain cell viability. Images were taken at 30-s intervals, and the permeability coefficients were calculated using the following equation (Adamson et al., 1994; Tran et al., 2020): $P = \frac{dI}{dt}\frac{r}{2I_o}$ where $dI/dt$ is the change in intensity over time, $r$ is radius of the blood vessel and $I_o$ is the maximum intensity.

## 2.9 | Oxygen consumption assay (OCR)

Oxygen consumption rate assay kits (Cayman Chemicals) were used to measure the relative amounts of oxygen consumed within each vessel condition. Due to the nature of the small cylindrical channels, we could not control the exact number of cells seeded within the channel for a given cell density injected into the device. Thus, to determine the number of cells lining the channel walls, DAPI images were obtained and cell nuclei were counted within each vessel condition. The cell densities for the OCR assays were then chosen to replicate these measurements: 10,000 cells/well as a reference, 129,408 cells/well (180-µm), 112,704 cells/well (300-µm, low density) and 175,296 cells/well (300-µm, high cell density). HCMEC/D3s were plated in a 96-well plate for 2 h to form a 2D monolayer, since the assay was not compatible with the 3D model. Once the monolayer was formed, culture medium supplemented with 10-µl of phosphorescent oxygen probe was added and oxygen consumption was measured over a time span of 30 min. These relative rates were then compared to previously published values to provide absolute quantities (McDonald et al., 2019; Sheikh et al., 2020).

### 2.10 | Computational modeling

To predict oxygen distributions within the hydrogel containing the 3D brain microvascular model, a finite element model was constructed using commercially available software (COMSOL). A schematic of the microfluidic device and the location of the collagen gel within the device is shown in Supporting Information: Figure S1a. The geometry of the collagen gel was imported into the finite element software and boundary conditions were applied. The cellular channel was modeled as a 5-μm-thick annulus as shown in Supporting Information: Figure S1b; the diameter of the acellular and cellular channels was set to either 180 or 300 μm depending on the experiment. A constitutive equation for Fick's second law was solved over the discretized geometry (triangular mesh elements):

$$\nabla \cdot \boldsymbol{J} = R, \quad (1)$$

where $\boldsymbol{J}$ is the flux vector and $R$ is the reaction rate.

Boundaries in direct contact with culture medium were set as fixed concentration to 21% oxygen (9.4 mol/m$^3$). The cellular annulus was set as a 0th-order volume reaction term with consumption rates obtained from the OCR for different cell seeding densities. The remaining boundaries were considered no flux (Supporting Information: Figure 1c). The oxygen diffusion coefficient was set at $4.5 \times 10^{-10}$ m$^2$/s within the collagen gel, using a value obtained from a previous study (Cheema et al., 2012).

In the hypoxic gradient experiments, when medium is perfused through the acellular channel, the boundary in the acellular channel is fixed at 9.4 mol/m$^3$. The Peclet number of the flow in the hypoxic gradient (300 μm diameter vessel and 5 μl/min flow rate) was approximately 8000, indicating convection dominates diffusion and the use of a constant concentration boundary condition.

### 2.11 | Statistics

Two-way analysis of variance (ANOVA) and post-hoc Tukey's HSD tests were performed to calculate statistical differences unless otherwise specified. For the hypoxic experiments, a Welch two sample *t*-test, assuming normal distributions with unequal variances between groups was used to calculate significant differences. P-value less than 0.05 indicated significant differences. Measurements from each condition were averaged from $n = 3$ or greater.

## 3 | RESULTS

### 3.1 | The effect of ECM composition and fluid flow on angiogenic sprouting

A primary advantage of the three-dimensional brain microvascular model is its ability to control specific biophysical variables to probe their effect on angiogenic sprouting. These studies interrogated the effects of both HA concentration in the collagen hydrogel and the application of fluid shear stress to the endothelial cells. Previous

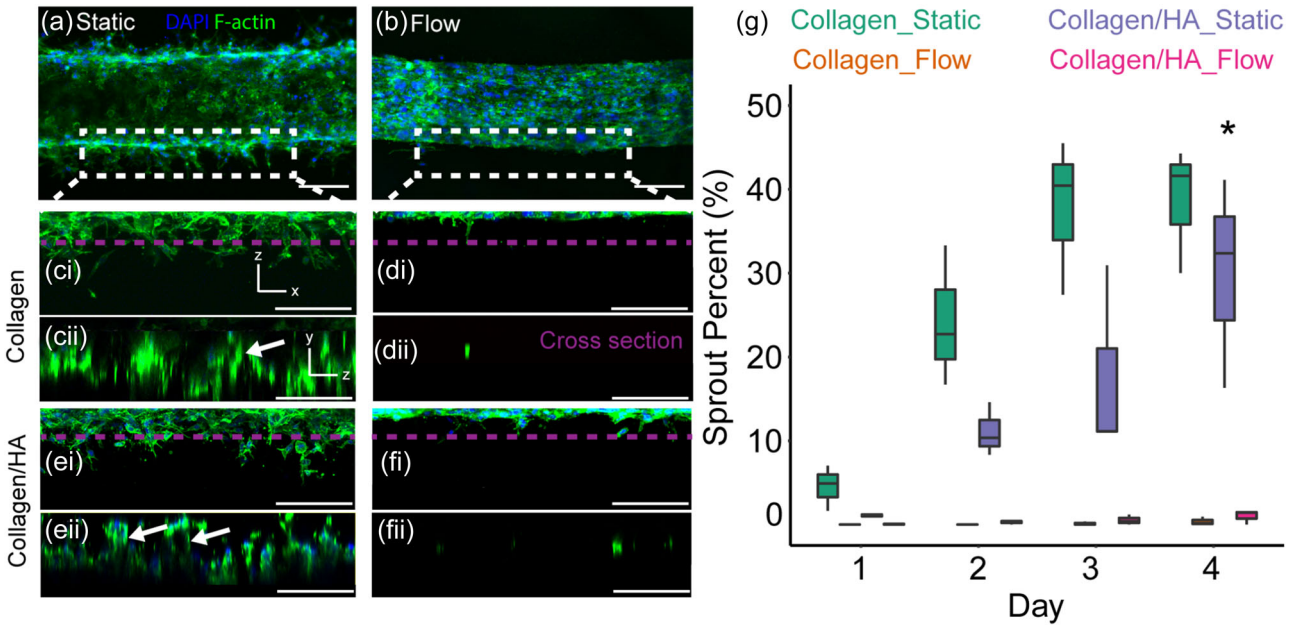


**FIGURE 1** One hundred and eighty micrometers blood vessels exposed to (a) static and (b) flow conditions after 4 days in culture. Angiogenic sprouts from 180-μm parent blood vessels fabricated in (c, d) collagen and (e, f) collagen/HA hydrogels on Day 4. (ci, ei) Blood vessels incubated in static conditions and (di, fi) vessels exposed to fluid flow. (ii) Confocal microscopy stacks of the YZ plane showing the presence of sprout lumens (white arrows). Purple dotted lines in c–f indicate the region of cross-section used for orthogonal views to identify the presence of luminal space within the angiogenic sprouts. (g) Sprouting percentage of the four conditions. DAPI = blue and F-actin = green. Scale = 100 μm. The box plots depict the median, 25 and 75 percentiles, and the whiskers represent 1.5x the interquartile range. *$p < 0.05$ ($n = 3$).

studies have shown that the addition of hyaluronan slows down the rate of polymerization of collagen hydrogels without affecting their equilibrium storage moduli, thus these experiments did not evaluate the effect of matrix mechanical properties on sprouting (Bowers et al., 2019). To quantify angiogenesis, a MATLAB code was written to measure the percentage of the vessel experiencing angiogenic sprouting for 4 days following cell seeding. Although maximum sprout length was initially calculated, sprouting frequency provided a more representative estimation of angiogenic activity along the length of the vessel in the bulk of the hydrogel. Figure 1a,b shows the entire 3D brain microvascular blood vessels exposed to static and flow conditions. Figure 1c,d focuses on the edge of phalloidin-stained vessels in collagen-only hydrogels after 4 days in two orthogonal planes. A shear stress of 0.7 dyn/cm$^2$ was chosen based on previous studies demonstrating this magnitude causes barriergenesis (Partyka et al., 2017) and is lower than the threshold that induces angiogenesis in HUVEC-lined channels (Galie et al., 2014). Shear stress substantially reduced sprouting from the vessel, though there were regions of the vessel exhibiting endothelial migration into the surrounding matrix (Figure 1d, ii). Figure 1c, ii (white arrow) shows the presence of small lumens in the sprouting structures in the static condition, indicative of early neovessel formation that is not observed in the flow condition (Figure 1b, ii). The addition of hyaluronan into the matrix did not affect sprouting in both static and flow conditions (Figure 1e,f). Again, only the static vessels featured lumens in the sprouting structures. Two-factor ANOVA analysis confirmed that the addition of flow but not hyaluronan significantly affected sprouting from the endothelial vessels (Figure 1g).

## 3.2 | Evaluating the effect of biophysical factors on oxygen concentration

In addition to exerting shear stress to the endothelial cells lining the vessel, the application of fluid flow also alters local oxygen tension by constantly replenishing the oxygen concentration within the cell-seeded channel. In static conditions, cellular oxygen consumption reduces the local oxygen concentrations. To determine whether the primary antiangiogenic effect of fluid flow is either by application of shear stress or by altering oxygen tension, endothelial cells were seeded within a larger diameter (300 µm) vessel. Increasing the diameter of the vessel reduces the volumetric density of the cells and mitigates local reduction in oxygen concentration. Therefore, an additional control was created by seeding these larger vessels with a higher concentration of cells, since recent studies have shown that altering radius of curvature can also dictate cell response (Bade et al., 2017). The cell number per unit area was quantified in the following six conditions: (i) 180-µm static, collagen-only, low seeding density, (ii) 180-µm flow, collagen-only, low seeding density, (iii) 180-µm static, collagen-HA, low seeding density, (iv) 180-µm flow, collagen-HA, low seeding density, (v) 300-µm static, collagen-only, low seeding density, and (vi) 300-µm static, collagen-only, high seeding density. Figure 2a,b shows DAPI stains of the walls of each of these vessels. One-way ANOVA and post-hoc Tukey comparisons indicated that the 300-µm high-density condition had a significantly higher density than the 300-µm low-density condition (Figure 2c). Images and quantification of DAPI within collagen/HA hydrogels reveal no significant difference between flow and static conditions (Supporting Information: Figure S2). To determine whether the difference in cell density also affected glucose levels, medium removed from the vessels was measured with a glucose sensor and indicated there was no significant differences between high and low cell density conditions (Supporting Information: Figure S3a). An OCR was then conducted on the cell density representing low density (112,704 cells/well) and high density (175,296 cells/well) as well as a density used in a previous study of HCMEC/D3 oxygen consumption that served as a reference value (McDonald et al., 2019; Sheikh et al., 2020). The consumption rates were measured to be $6.4 \times 10^{-11}$ mol/min and $9.6 \times 10^{-11}$ mol/min for the low and high densities respectively (Supporting Information: Figure S3b,c).

The consumption rates were then incorporated into a finite element model as a reaction term in the diffusion constitutive equation for different cell densities. Figure 2d shows contour maps of oxygen tension for 180-µm vessels in static and flow conditions and 300-µm vessels with low and high seeding densities. Supporting Information: Figure S4 demonstrates that the oxygen gradient is mostly constant along the length of the channel in the bulk of the hydrogel where measurements were taken. The HA-containing vessels weren't modeled since the presence of HA did not significantly affect cell density. The predicted oxygen tensions surrounding the vessels indicated substantial differences based on vessel radius and the application of shear stress. As expected, applying flow maintains the oxygen levels at ambient levels, and the larger diameter vessel mitigates the oxygen reduction for a given cell density. Figure 2e shows that the high cell density increases the oxygen deficit in the 300-µm vessel, but not to the level of the 180-µm vessel exposed to static conditions. Given the large difference in oxygen concentration between the 300-µm high density and low-density vessels, sprouting density was evaluated in these two conditions. Figure 2f shows there is substantially more sprouting in the high-density vessel, and one-factor ANOVA reveals that the cell density significantly affects sprouting percentage (Figure 2g). Moreover, the 180-µm static vessel, which the finite element model predicted to have the lowest local oxygen concentrations, had significantly greater sprouting than both the high and low cell density 300-µm vessels (Supporting Information: Figure S5). Combined with the results presented in Figure 1, these results suggest a direct correlation between reduced oxygen levels and increased angiogenic response.

## 3.3 | Differentiating between the effects of oxygen concentration and oxygen gradient

To determine whether hypoxia is the driving factor for angiogenesis in the 3D brain microvascular model, 300-µm vessels with low cell

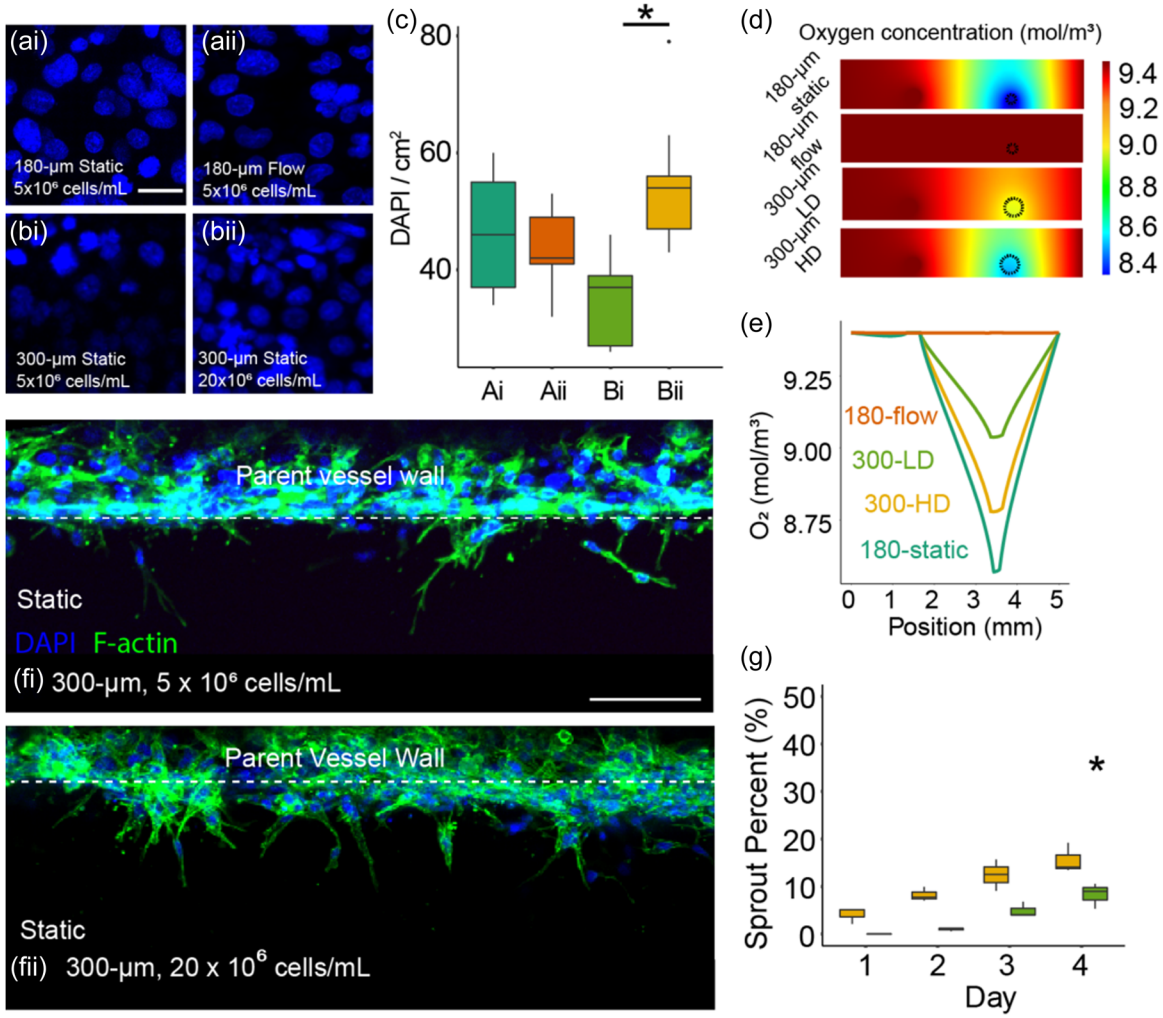


**FIGURE 2** Confocal images of DAPI stains verifying cells per area in (a) 180-µm seeded with $5 \times 10^6$ cells/ml in collagen-only hydrogels exposed to (i) static and (ii) flow conditions and (b) 300-µm collagen-only hydrogels seeded with (i) $5 \times 10^6$ cells/ml and (ii) $20 \times 10^6$ cells/ml. (c) Quantification of nuclei per 1 $cm^2$. (d) Computational models of oxygen consumption in each vessel conditions. Scale = 100 µm. (e) Oxygen levels dependent on distance from vessels, *y*-axis range is 8.5-9.5 $mol/m^3$. (f) Immunofluorescence images of angiogenic sprouts in 300-µm seeded with (i) $5 \times 10^6$ cells/ml and (ii) $20 \times 10^6$ cells/ml. (g) Sprouting percentage of these conditions. DAPI = blue and F-actin = green. Scale = 50 µm. The box plots depict the median, 25 and 75 percentiles, and the whiskers represent 1.5x the interquartile range. $^*p < 0.05$ ($n = 3$).

seeding density were incubated in a hypoxic chamber for 4 days before measuring angiogenic sprouting. As shown in Figure 2f, not only is the oxygen concentration reduced in the conditions exhibiting increased sprouting, but the oxygen gradient is also increased. Therefore, a second condition was tested by imposing an external oxygen gradient to the vessel: oxygenated medium was perfused through the channel adjacent to the endothelialized channel while the device was in the hypoxic chamber. To verify that application of flow through the acellular channel did not cause interstitial pressure gradients across the cell-seeded channel, the fluid dynamics were assessed by modeling the collagen gel as a porous medium (Galie et al., 2012). Supporting Information: Figure S6 indicates that there is a negligible interstitial pressure gradient caused by perfusion through the acellular channel. Schematics in Figure 3a, display the differences between the hypoxic (i) and oxygen gradient (ii) conditions. Figure 3b shows that minimal sprouting was observed in blood vessels exposed to a constant 1% $O_2$ environment after 4 days. In contrast, the channels with the external oxygen gradient exhibited substantial sprouting along the length of the vessel (Figure 3c). Quantification revealed that blood vessels in the constant hypoxic environment exhibited significantly lower sprout percentages compared to the $O_2$ gradient condition (Figure 3d). The finite element model provided a means to estimate the difference in oxygen gradients between conditions. Figure 3e shows contour plots between the hypoxic and gradient conditions, and Figure 3f provides quantification of the spatial oxygen gradient for these two conditions as well as the 300-µm low-density vessels in normoxic conditions. The plot shows that despite the large difference in absolute oxygen concentrations, there is a negligible difference in the oxygen gradient between normoxic and hypoxic conditions (~200 $mol/m^3/m$) compared to the imposed gradient, which is approximately an order of magnitude greater. Overall, these results demonstrate that the

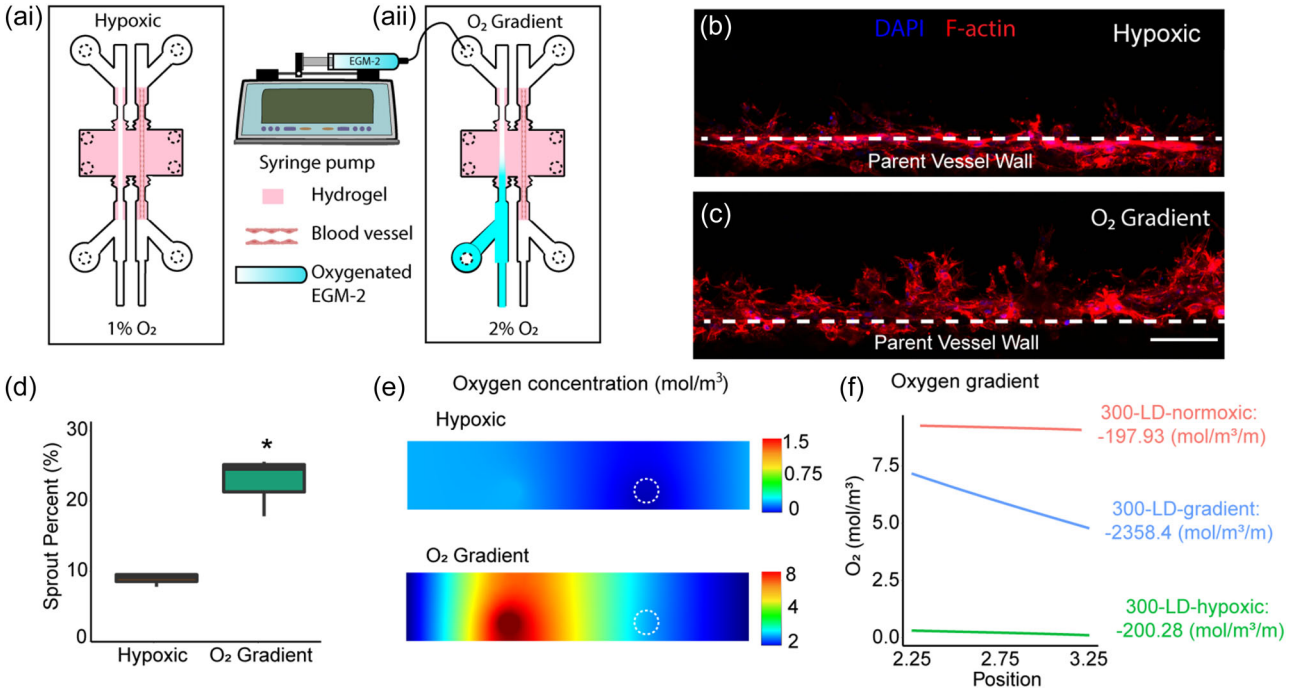


**FIGURE 3** Schematic of blood vessels in static conditions incubated in a hypoxic and oxygen gradient environment. Confocal images of angiogenic sprouts in 300-μm vessels seeded with $5 \times 10^6$ cells/ml exposed to (b) hypoxia and (c) $O_2$ gradient. (d) Quantification of sprout percentage. (e) Computational models of oxygen concentration in each vessel conditions. (f) Oxygen levels dependent on distance from vessels. DAPI = blue and F-actin = red. Scale = 100 μm. The box plots depict the median, 25 and 75 percentiles, and the whiskers represent 1.5x the interquartile range. $^*p < 0.05$ ($n = 3$).

oxygen gradient is the main driving factor for angiogenesis and that the biophysical factors that affected sprouting, flow, and radius of curvature, did so primarily through their effects on the oxygen gradient experienced by cells lining the vessel.

### 3.4 | Evaluating the influence of oxygen gradients on barriergenesis

The importance of oxygen gradient on barrier formation was also evaluated in the 3D brain microvascular model. Previous studies have found that fluid flow is required for barrier formation, with the assumption that the shear stress exerted by the fluid flow was the primary factor for barriergenesis. Given the result that fluid flow also altered the oxygen gradient, the barrier integrity of several conditions with varying angiogenic responses (180-μm static with and without HA, 180-μm flow with and without HA, and 300-μm low density) were evaluated to interrogate any potential correlation between oxygen levels and tight junction formation. The vessels exposed to static conditions exhibited no significant difference in either ZO-1 localization to the cell-cell junctions (Figure 4a–c) or in the permeability of 4-kDa FITC dextran (Figure 4d), despite large differences in sprouting caused by the difference in vessel diameter. Moreover, the 180-μm vessels exposed to flow exhibited substantially lower vessel permeabilities. There was increased ZO-1 localization to cell–cell junctions (Figure 4e,f) and the permeability was significantly lower than the static values (Figure 4g). In contrast to the static conditions, there was a significant difference between the flow conditions with and without HA: incorporation of HA significantly reduced the permeability, despite not having any effect on oxygen gradient and angiogenic sprouting. The ZO-1 images and permeability assays are consistent with previous results showing that CD44 mediates shear stress mechanotransduction through small GTPases such as RhoA and Rac1 to induce barriergenesis in cerebral vasculature (DeOre et al., 2022). Moreover, ZO-1 was present in the sprouts from both static and flow conditions, but it was not localized to the cell–cell junctions in either condition (Supporting Information: Figure S7). This result is consistent with the permeability measurements, since parent vessels did not exhibit barrier function in the static condition and there were no lumens observed in the sprouts from parent vessels exposed to flow. Overall, these results demonstrate no correlation between oxygen gradient and barrier integrity and supports the hypothesis that the mechanical stress exerted by fluid flow is the primary factor driving barrier formation in the 3D brain microvascular model. Taken together with the data presented in Figure 1 that vessels exposed to flow exhibit a nonzero level of angiogenic sprouting, these results suggest that the mechanisms dictating angiogenesis and barriergenesis are independent from one another and sprouting does not compromise the barrier.

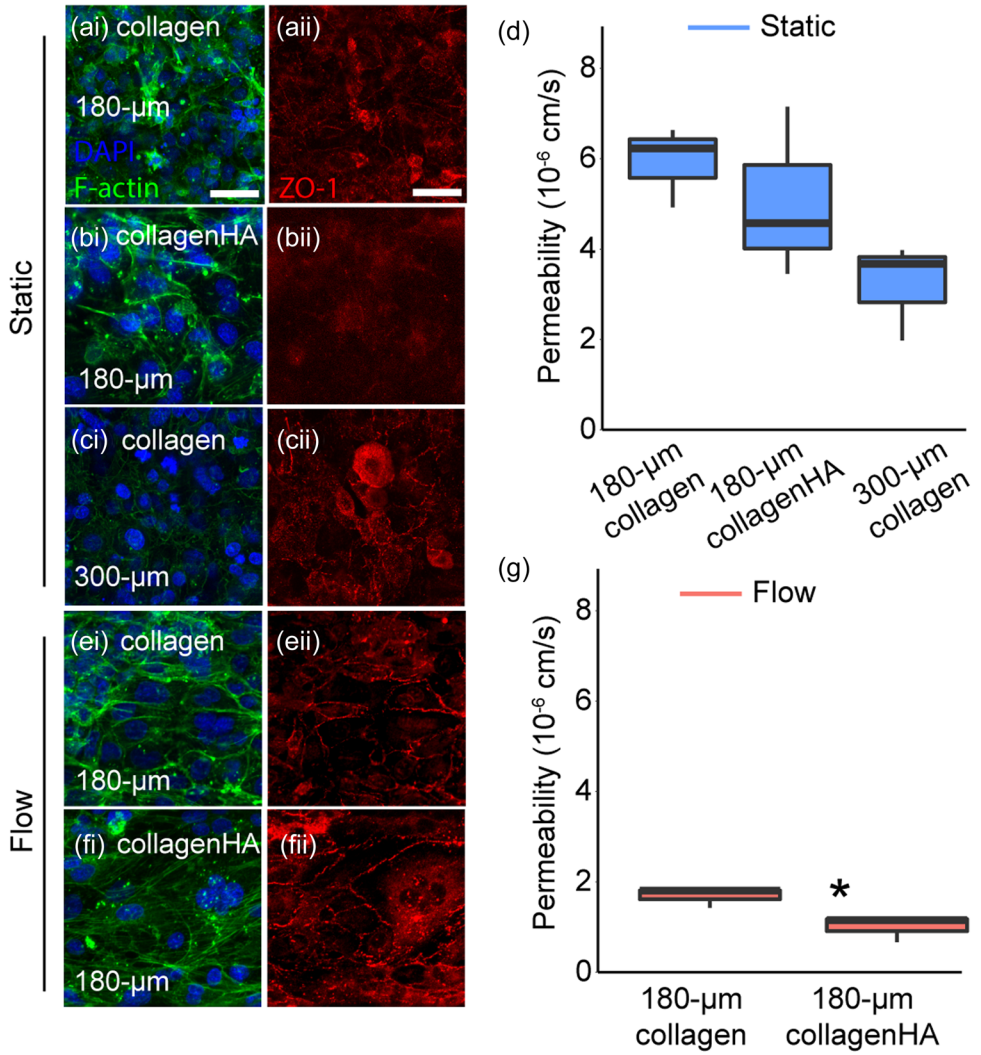


**FIGURE 4** (a–c) Confocal stacks of blood vessels cultured in static conditions and (e,f) flow conditions labeled with (i) DAPI (blue), FITC-phalloidin (green), and (ii) ZO-1 (red). Permeability quantification of vessels exposed to (d) static and (g) luminal shear stress for 4 days measured with 4 kDa dextran. Scale = 50 μm. The box plots depict the median, 25 and 75 percentiles, and the whiskers represent 1.5x the interquartile range. $^*p < 0.05$ ($n = 3$).

## 4 | DISCUSSION

The combination of experimental and computational results presented here identify the spatial oxygen gradient as the primary instigating factor for angiogenic sprouting in cerebral vasculature among the biophysical parameters evaluated here: matrix composition, fluid shear stress, and vessel diameter. The relationship between oxygen concentration and angiogenesis has been cited frequently, especially in the context of tumor formation where hypoxia and formation of neovessels are spatially correlated. However, there is ample evidence that the connection between oxygen concentration and angiogenesis may be more complex than a direct causal link: previous studies have shown that hypoxia does not always correlate to the growth of new blood vessels from existing vasculature (Moeller et al., 2004). Several tissues including the myocardium (Moss, 1968) and visual cortex (Padnick et al., 1999) have baseline, physiologic hypoxia that do not induce angiogenesis. Moreover, there are processes like wound healing where hypoxia is a byproduct of angiogenesis, not a driving factor (Moeller et al., 2004). The in vitro 3D brain microvascular model presents a means to directly evaluate the effect of hypoxia in cerebral vasculature, and it demonstrated no significant difference in sprouting between normoxic conditions and an environment with 1% oxygen. In contrast, imposing an external oxygen gradient by perfusing oxygenated medium through an adjacent channel in low oxygen ambient conditions significantly increased angiogenic sprouting. Taken together, these results show that simply decreasing the oxygen levels does not lead to activation of endothelial cells, but rather the presence of a gradient may lead to angiogenesis.

Further studies are required to clarify whether the effect of oxygen gradient on angiogenesis is unique to the central nervous system. Endothelial cells in the brain have unique properties, including the formation of tight junctions that give rise to the

blood-brain barrier. Their metabolic activities also differ from other regions of the body, and therefore these cells may respond to oxygen levels differently from their counterparts in other organs. There are several pathologies where large oxygen gradients are present within the central nervous system, and these scenarios are characterized by rapid angiogenesis. For example, the formation of glioblastoma (GBM) creates large spatial gradients of oxygen between the tumor and surrounding parenchyma, and GBM exhibits substantial growth of new vessels from the existing vasculature [36–37]. Moreover, following spinal cord injury there is a strong and temporary angiogenic response that precedes the formation of a glial scar (Dray et al., 2009), and the site of injury is characterized by hypoxia due to disruption of the blood supply. The result that oxygen gradient is the primary driving factor for angiogenesis in the central nervous system is consistent with these pathologies. There are several examples of pathologies outside the central nervous system, including tumor formation and wound healing, that suggest the effect of oxygen gradient is universal. In vitro vascular models provide a means to evaluate the relationship between spatial differences in oxygen levels and angiogenesis in other organ systems.

The effect of oxygen gradients on barrier formation was also evaluated, given the ability of cerebral endothelial cells to form tight junctions. In contrast to angiogenesis, there did not appear to be a correlation between oxygen gradient and the barrier integrity of the 3D vessels. Both the low density, 300-µm diameter vessel cultured in static conditions and the 180-µm diameter vessel perfused with 0.7 dyn/cm$^2$ of shear stress exhibited the two lowest oxygen gradients of the conditions tested, and these conditions had significantly different permeabilities and localization of ZO-1 to cell-cell junctions. As shown in a previous version of this 3D blood-brain barrier model (Partyka et al., 2017), the main driving factor for barrier formation is the shear stress exerted on the endothelium by fluid flow, and these results are consistent with that finding. These studies indicate that different stimuli and likely different signaling pathways mediate barrier formation and angiogenic sprouting. Given that the vessels exposed to flow exhibited some level of sprouting, though significantly less than other conditions, the two processes of barrier formation and angiogenesis may occur simultaneously. In fact, a recent study using transgenic zebrafish with promoters for barrier development demonstrated that angiogenesis and barriergenesis occur at the same time within the central nervous system (Umans et al., 2017). Additional studies are required to understand the interdependence, or lack thereof, of signaling pathways mediating these two processes.

The results of the study do not preclude the importance of other proangiogenic factors unrelated to the spatial oxygen gradient. Although noncerebral endothelial cells were used, previous *in vitro* models have identified the growth factors most likely to stimulate sprouting from an endothelialized vessel (Nguyen et al., 2013). Small GTPases like cdc42 that contribute to sprouting are activated by specific agonists and not differences in oxygen concentration (Nguyen et al., 2017). Furthermore, previous studies have shown that fluid shear stress, if applied with a sufficiently high magnitude, can induce sprouting from HUVEC-lined channels with diameters of 400-µm (Galie et al., 2014). Augmenting shear stress by increasing flow rate does not exacerbate the oxygen gradient experienced by the cells within the vessel, suggesting that the mechanical stimulus is responsible for instigating angiogenesis. Overall, there are likely several biophysical and biochemical factors that cause sprouting independent of local oxygen levels. Nonetheless, the studies presented here reveal that oxygen gradient is more important than overall oxygen concentration for driving angiogenesis.

## CONFLICT OF INTEREST

The authors declare no conflict of interest.

## ORCID

*Kiet A. Tran* https://orcid.org/0000-0002-8388-2912

## REFERENCES

Adamson, R. H., Lenz, J. F., & Curry, F. E. (1994). Quantitative laser scanning confocal microscopy on single capillaries: Permeability measurement. *Microcirculation*, *1*(4), 251–265. https://doi.org/10.3109/10739689409146752

Alberding, J. P., & Secomb, T. W. (2021). Simulation of angiogenesis in three dimensions: Application to cerebral cortex. *PLoS Computational Biology*, *17*(6), e1009164. https://doi.org/10.1371/journal.pcbi.1009164

Azimzadeh, M., Khashayar, P., Amereh, M., Tasnim, N., Hoorfar, M., & Akbari, M. (2021). Microfluidic-based oxygen ($O_2$) sensors for on-chip monitoring of cell, tissue and organ metabolism. *Biosensors*, *12*(1), 6. https://doi.org/10.3390/bios12010006

Bade, N. D., Kamien, R. D., Assoian, R. K., & Stebe, K. J. (2017). Curvature and rho activation differentially control the alignment of cells and stress fibers. *Science Advances*, *3*(9), e1700150. https://doi.org/10.1126/sciadv.1700150

Bowers, H. C., Fiori, M. L., Khadela, J. B., Janmey, P. A., & Galie, P. A. (2019). Cell-matrix tension contributes to hypoxia in astrocyte-seeded viscoelastic hydrogels composed of collagen and hyaluronan. *Experimental Cell Research*, *376*(1), 49–57. https://doi.org/10.1016/j.yexcr.2019.01.012

Caja, S., & Enríquez, J. A. (2017). Mitochondria in endothelial cells: Sensors and integrators of environmental cues. *Redox Biology*, *12*, 821–827. https://doi.org/10.1016/j.redox.2017.04.021

Cheema, U., Rong, Z., Kirresh, O., MacRobert, A. J., Vadgama, P., & Brown, R. A. (2012). Oxygen diffusion through collagen scaffolds at defined densities: Implications for cell survival in tissue models. *Journal of Tissue Engineering and Regenerative Medicine*, *6*(1), 77–84. https://doi.org/10.1002/term.402

Clifford, P. M., Zarrabi, S., Siu, G., Kinsler, K. J., Kosciuk, M. C., Venkataraman, V., D'Andrea, M. R., Dinsmore, S., & Nagele, R. G. (2007). Aβ peptides can enter the brain through a defective blood-brain barrier and bind selectively to neurons. *Brain Research*, *1142*(1), 223–236. https://doi.org/10.1016/j.brainres.2007.01.070

Deore, B. J., Partyka, P. P., Fan, F., & Galie, P. A. (2022). CD44 mediates shear stress mechanotransduction in an in vitro blood-brain barrier model through small GTPases RhoA and Rac1. *The FASEB Journal*, *36*(5), e22278. https://doi.org/10.1096/fj.202100822RR

Doddaballapur, A., Michalik, K. M., Manavski, Y., Lucas, T., Houtkooper, R. H., You, X., Chen, W., Zeiher, A. M., Potente, M., Dimmeler, S., & Boon, R. A. (2015). Laminar shear stress inhibits endothelial cell metabolism via KLF2-mediated repression of PFKFB3. *Arteriosclerosis, Thrombosis, and Vascular Biology*, *35*(1), 137–145. https://doi.org/10.1161/ATVBAHA.114.304277

Dray, C., Rougon, G., & Debarbieux, F. (2009). Quantitative analysis by in vivo imaging of the dynamics of vascular and axonal networks in injured mouse spinal cord. *Proceedings of the National Academy of Sciences*, *106*(23), 9459–9464. https://doi.org/10.1073/pnas.0900222106

Galie, P. A., Byfield, F. J., Chen, C. S., Kresh, J. Y., & Janmey, P. A. (2015). Mechanically stimulated contraction of engineered cardiac constructs using a microcantilever. *IEEE Transactions on Biomedical Engineering*, *62*(2), 438–442. https://doi.org/10.1109/TBME.2014.2357778

Galie, P. A., Nguyen, D. -H. T., Choi, C. K., Cohen, D. M., Janmey, P. A., & Chen, C. S. (2014). Fluid shear stress threshold regulates angiogenic sprouting. *Proceedings of the National Academy of Sciences*, *111*(22), 7968–7973. https://doi.org/10.1073/pnas.1310842111

Galie, P. A., Russell, M. W., Westfall, M. V., & Stegemann, J. P. (2012). Interstitial fluid flow and cyclic strain differentially regulate cardiac fibroblast activation via AT1R and TGF-β1. *Experimental Cell Research*, *318*(1), 75–84. https://doi.org/10.1016/j.yexcr.2011.10.008

Halder, S. K., & Milner, R. (2020). Mild hypoxia triggers transient blood–brain barrier disruption: A fundamental protective role for microglia. *Acta Neuropathologica Communications*, *8*(1), 175. https://doi.org/10.1186/s40478-020-01051-z

Hickey, M. M., & Simon, M. C. (2006). Regulation of angiogenesis by hypoxia and hypoxia-inducible factors. *Current Topics in Developmental Biology*, *76*, 217–257. https://doi.org/10.1016/S0070-2153(06)76007-0

Hormuth, D. A., Phillips, C. M., Wu, C., Lima, E. A. B. F., Lorenzo, G., Jha, P. K., Jarrett, A. M., Oden, J. T., & Yankeelov, T. E. (2021). Biologically-based mathematical modeling of tumor vasculature and angiogenesis via time-resolved imaging data. *Cancers*, *13*(12), 3008. https://doi.org/10.3390/cancers13123008

Kim, S., Chung, M., Ahn, J., Lee, S., & Jeon, N. L. (2016). Interstitial flow regulates the angiogenic response and phenotype of endothelial cells in a 3D culture model. *Lab on a Chip*, *16*(21), 4189–4199. https://doi.org/10.1039/c6lc00910g

Lee, G., Huang, S. A., Aw, W. Y., Rathod, M. L., Cho, C., Ligler, F. S., & Polacheck, W. J. (2022). Multilayer microfluidic platform for the study of luminal, transmural, and interstitial flow. *Biofabrication*, *14*(2), 025007. https://doi.org/10.1088/1758-5090/ac48e5

McDonald, C., Drewes, L., & Blankenheim, Z. (2019). Brain endothelial cell bioenergetics via extracellular flux analysis. *The FASEB Journal*, *33*(S1). https://doi.org/10.1096/fasebj.2019.33.1_supplement.708.1

Moeller, B. J., Cao, Y., Vujaskovic, Z., Li, C. Y., Haroon, Z. A., & Dewhirst, M. W. (2004). The relationship between hypoxia and angiogenesis. *Seminars in Radiation Oncology*, *14*(3), 215–221. https://doi.org/10.1016/j.semradonc.2004.04.005

Moss, A. J. (1968). Intramyocardial oxygen tension. *Cardiovascular Research*, *2*(3), 314–318. https://doi.org/10.1093/cvr/2.3.314

Nguyen, D. H. T., Gao, L., Wong, A., & Chen, C. S. (2017). Cdc42 regulates branching in angiogenic sprouting in vitro. *Microcirculation*, *24*(5). https://doi.org/10.1111/micc.12372

Nguyen, D. H. T., Stapleton, S. C., Yang, M. T., Cha, S. S., Choi, C. K., Galie, P. A., & Chen, C. S. (2013). Biomimetic model to reconstitute angiogenic sprouting morphogenesis in vitro. *Proceedings of the National Academy of Sciences of the United States of America*, *110*(17), 6712–6717. https://doi.org/10.1073/pnas.1221526110

Niu, G., & Chen, X. (2010). Vascular endothelial growth factor as an anti-angiogenic target for cancer therapy. *Current Drug Targets*, *11*(8), 1000–1017. https://doi.org/10.2174/138945010791591395

Padnick, L. B., Linsenmeier, R. A., & Goldstick, T. K. (1999). Oxygenation of the cat primary visual cortex. *Journal of Applied Physiology*, *86*(5), 1490–1496. https://doi.org/10.1152/jappl.1999.86.5.1490

Partyka, P. P., Godsey, G. A., Galie, J. R., Kosciuk, M. C., Acharya, N. K., Nagele, R. G., & Galie, P. A. (2017). Mechanical stress regulates transport in a compliant 3D model of the blood-brain barrier. *Biomaterials*, *115*, 30–39. https://doi.org/10.1016/j.biomaterials.2016.11.012

Placone, A. L., McGuiggan, P. M., Bergles, D. E., Guerrero-Cazares, H., Quiñones-Hinojosa, A., & Searson, P. C. (2015). Human astrocytes develop physiological morphology and remain quiescent in a novel 3D matrix. *Biomaterials*, *42*, 134–143. https://doi.org/10.1016/j.biomaterials.2014.11.046

Polacheck, W. J., Kutys, M. L., Tefft, J. B., & Chen, C. S. (2019). Microfabricated blood vessels for modeling the vascular transport barrier. *Nature Protocols*, *14*(5), 1425–1454. https://doi.org/10.1038/s41596-019-0144-8

Rellick, S. L., Hu, H., Simpkins, J. W., & Ren, X. (2016). Evaluation of bioenergetic function in cerebral vascular endothelial cells. *Journal of Visualized Experiments*, *2016*(117), 54847. https://doi.org/10.3791/54847

Rink, C., & Khanna, S. (2011). Significance of brain tissue oxygenation and the arachidonic acid cascade in stroke. *Antioxidants and Redox Signaling*, *14*(10), 1889–1903. https://doi.org/10.1089/ars.2010.3474

Sheikh, M. H., Henson, S. M., Loiola, R. A., Mercurio, S., Colamatteo, A., Maniscalco, G. T., de Rosa, V., McArthur, S., & Solito, E. (2020). Immuno-metabolic impact of the multiple sclerosis patients' sera on endothelial cells of the blood-brain barrier. *Journal of Neuroinflammation*, *17*, 153. https://doi.org/10.1186/s12974-020-01810-8

Song, J. W., Daubriac, J., Tse, J. M., Bazou, D., & Munn, L. L. (2012). RhoA mediates flow-induced endothelial sprouting in a 3-D tissue analogue of angiogenesis. *Lab on a Chip*, *12*(23), 5000–5006. https://doi.org/10.1039/c2lc40389g

Tran, K. A., Partyka, P. P., Jin, Y., Bouyer, J., Fischer, I., & Galie, P. A. (2020). Vascularization of self-assembled peptide scaffolds for spinal cord injury repair. *Acta Biomaterialia*, *104*, 76–84. https://doi.org/10.1016/j.actbio.2019.12.033

Umans, R. A., Henson, H. E., Mu, F., Parupalli, C., Ju, B., Peters, J. L., Lanham, K. A., Plavicki, J. S., & Taylor, M. R. (2017). CNS angiogenesis and barriergenesis occur simultaneously. *Developmental Biology*, *425*(2), 101–108. https://doi.org/10.1016/j.ydbio.2017.03.017

Vilanova, G., Burés, M., Colominas, I., & Gomez, H. (2018). Computational modelling suggests complex interactions between interstitial flow and tumour angiogenesis. *Journal of the Royal Society Interface*, *15*(146); 20180415. https://doi.org/10.1098/rsif.2018.0415

van Duinen, V., Zhu, D., Ramakers, C., van Zonneveld, A. J., Vulto, P., & Hankemeier, T. (2019). Perfused 3D angiogenic sprouting in a high-throughput in vitro platform. *Angiogenesis*, *22*(1), 157–165. https://doi.org/10.1007/s10456-018-9647-0

Wang, W. Y., Jarman, E. H., Lin, D., & Baker, B. M. (2021). Dynamic endothelial stalk cell-matrix interactions regulate angiogenic sprout diameter. *Frontiers in Bioengineering and Biotechnology*, *9*, 620128. https://doi.org/10.3389/fbioe.2021.620128

Wang, W. Y., Kent, R. N., Huang, S. A., Jarman, E. H., Shikanov, E. H., Davidson, C. D., Hiraki, H. L., Lin, D., Wall, M. A., Matera, D. L., Shin, J. W., Polacheck, W. J., Shikanov, A., & Baker, B. M. (2021). Direct comparison of angiogenesis in natural and synthetic biomaterials reveals that matrix porosity regulates endothelial cell invasion speed and sprout diameter. *Acta Biomaterialia*, *135*, 260–273. https://doi.org/10.1016/j.actbio.2021.08.038

Watts, M. E., Pocock, R., & Claudianos, C. (2018). Brain energy and oxygen metabolism: Emerging role in normal function and disease. *Frontiers in Molecular Neuroscience*, *11*, 216. https://doi.org/10.3389/fnmol.2018.00216

Weksler, B. B. (2005). Blood-brain barrier-specific properties of a human adult brain endothelial cell line. *The FASEB Journal*, *26*, 1–26. https://doi.org/10.1096/fj.04-3458fje

Williams, P. A., Stilhano, R. S., To, V. P., Tran, L., Wong, K., & Silva, E. A. (2015). Hypoxia augments outgrowth endothelial cell (OEC)

sprouting and directed migration in response to sphingosine-1-phosphate (S1P). *PLoS One*, *10*(4), e0123437. https://doi.org/10.1371/journal.pone.0123437

Winkelman, M. A., Kim, D. Y., Kakarla, S., Grath, A., Silvia, N., & Dai, G. (2022). Interstitial flow enhances the formation, connectivity, and function of 3D brain microvascular networks generated within a microfluidic device. *Lab on a Chip*, *22*(1), 170–192. https://doi.org/10.1039/d1lc00605c

Yetkin-Arik, B., Vogels, I. M. C., Nowak-Sliwinska, P., Weiss, A., Houtkooper, R. H., Van Noorden, C. J. F., Klaassen, I., & Schlingemann, R. O. (2019). The role of glycolysis and mitochondrial respiration in the formation and functioning of endothelial tip cells during angiogenesis. *Scientific Reports*, *9*(1), 12608. https://doi.org/10.1038/s41598-019-48676-2

## SUPPORTING INFORMATION

Additional supporting information can be found online in the Supporting Information section at the end of this article.

**How to cite this article:** Tran, K. A., Baldwin-LeClair, A., DeOre, B. J., Antisell, M., & Galie, P. A. (2022). Oxygen gradients dictate angiogenesis but not barriergenesis in a 3D brain microvascular model. *Journal of Cellular Physiology*, 1–11. https://doi.org/10.1002/jcp.30840